Chemical Science

RSCPublishing

EDGE ARTICLE

View Article Online
View Journal

Cite this: DOI: 10.1039/c3sc52344f

Structure–property relationships for 1,7-diphenoxy-perylene bisimides in solution and in the solid state†

Ángel J. Jiménez,[a] Mei-Jin Lin,[a] Christian Burschka,[a] Johannes Becker,[b] Volker Settels,[b] Bernd Engels[b] and Frank Würthner*[a]

Received 21st August 2013
Accepted 3rd October 2013

DOI: 10.1039/c3sc52344f

www.rsc.org/chemicalscience

To elucidate the impact of widely employed solubilizing phenoxy substituents on the structural and functional properties of perylene bisimide (PBI) dyes a series of 1,7-diphenoxy-substituted PBIs was prepared from 1,7-dibromo PBI which exhibit hydrogen, methyl, isopropyl or phenyl substituents at one or both *ortho* positions of the phenoxy substituents. Despite increasing sterical congestion high yields of 74–88% could be obtained for all twofold aromatic nucleophilic substitution reactions. The structural and optical properties in solution and in the solid state were investigated by ^{1}H NMR, UV-Vis absorption and fluorescence spectroscopy, single crystal X-ray analyses (four structures) as well as quantum chemical and force field calculations. For the latter we used an adapted force field which correctly reflects the rigidity of the PBI core. Our studies show that these dyes prefer to accommodate a slightly twisted molecular structure in solution that is supported by CH⋯O hydrogen bonds between the 1,7-oxygen and the 6,12-hydrogen substituents. Because of the rather shallow potential energy surface, however, the molecules may planarize in the crystalline state under the influence of packing forces as revealed by single crystal X-ray analyses for two derivatives bearing methyl or phenyl substituents at all phenoxy *ortho*-positions. Such substituents are also suited to enwrap the PBI π-scaffold and to prohibit PBI aggregation in the bulk state giving rise to defined vibronic progressions in the solid state UV-Vis absorption and emission spectra, and appreciable fluorescence quantum yields of up to 37%. In dichloromethane solution all of these 1,7-diphenoxy-substituted PBI dyes exhibit fluorescence quantum yields of 98–100% despite significant differences in the shape of the UV-Vis absorption band. The latter was explained in terms of rigidity because the molecules bearing four *ortho*-substituents at the phenoxy substituents were shown to prevail in much more fixed conformations compared to their more simple counterparts. Our findings underline that the conformational flexibility of bay-substituents can have an important impact on the functional properties of PBI dyes.

Introduction

For π-conjugated molecules it is common practice to assume planar structures as long as no bulky substituents require distortions of the molecular scaffolds.[1] This holds particularly true for polycyclic aromatic hydrocarbons formed by annulation of benzene rings[2] owing to the gain in resonance energy by means of delocalized π-electrons. On the other hand, in the presence of sterical congestion due to bulky substituents, the aromatic π-scaffolds are expected to distort to the extent required to accommodate these substituents. If available, crystallographic data are taken as unambiguous evidence for the prevailing molecular structures and the impact of packing effects on the distortion is widely ignored.

This way of thinking has also been applied to perylene bisimide (PBI) dyes[3] bearing substituents in the sterically demanding 1,6,7,12-positions, the so-called bay area.[4] Extensive work on this class of dyes with carbon, nitrogen, oxygen or halogen substituents at the bay positions and the availability of more than a dozen crystal structures[5] pointed to the fact that the energetic penalty associated with the distortion of the π-scaffold cannot be as high as is widely assumed and showed that already minor sterical encumbering or presumably even packing effects may twist the π-scaffold out of planarity. The effect of sterical encumbering at the bay positions is nicely illustrated by the crystal structures of 1,6,7,12-tetrachloro[6] and 1,2,5,6,7,8,11,12-octachloro PBIs,[7] which show that two naphthalene imide units are twisted by 36.7° and 35.8°, respectively, at the central six-membered ring. Even more distorted PBI

---

[a] *Universität Würzburg, Institut für Organische Chemie & Center for Nanosystems Chemistry, Am Hubland, 97074 Würzburg, Germany. E-mail: wuerthner@chemie.uni-wuerzburg.de; Fax: +49-931-31-84756; Tel: +49-931-31-85340*

[b] *Universität Würzburg, Institut für Physikalische und Theoretische Chemie, Am Hubland, 97074 Würzburg, Germany*

† Electronic supplementary information (ESI) available: Synthesis, ^{1}H and ^{13}C NMR spectra, UV-Vis and fluorescence spectra, theoretical calculations and crystallographic data. CCDC 952111–952113. For ESI and crystallographic data in CIF or other electronic format see DOI: 10.1039/c3sc52344f

scaffolds have been revealed by Wang and coworkers upon annulation of two or three PBIs at the bay positions to give laterally fused PBI oligomers.[8] Similarly for other classes of polycyclic aromatic hydrocarbons preferential bending upon sterical congestion has been observed as well, *e.g.* for helicenes,[9] acenes,[10] hexabenzocoronenes[11] and dibenzotetrathienocoronenes,[12] and π-expanded cyclooctatetraenes.[13]

Several of the above mentioned investigations showed the important interrelationship of molecular structure and packing arrangements with regard to the functional properties such as fluorescence,[14] electroluminescence,[15] charge transport[16] and photovoltaic properties[17] arising in bulk materials. For instance, distorted bay-substituted PBIs could be packed in slipped arrangements with the aid of hydrogen-bonding to give superb n-channel transistors[7] and the distortion of dibenzotetrathienocoronenes was shown to support the formation of improved interfaces with C_{60} (ref. 12) and C_{70} (ref. 18) fullerenes for photovoltaics. In this context it appears highly desirable to estimate possible distortions of molecular geometries (which nowadays can easily be calculated by quantum chemical methods) and energetic balances associated with crystal packing.[10,19]

For our study, we used 1,7-diphenoxy-substituted PBIs, which are among the most widely utilized PBI scaffolds due to the easy synthesis *via* bromination and nucleophilic displacement reactions.[20] Although no crystallographic data were available until recently, it was commonly assumed that the bay area suffers from sterical encumbering and accordingly a torsional twist between 5 and 10° should originate as observed in the crystal structures of other 1,7-disubstituted PBIs.[21] In this regard we were surprised when the crystal structure of 1,7-bis-(2,6-diphenylphenoxy)-PBI revealed a planar PBI π-scaffold in the solid state.[22] Likewise the well-defined vibronic progressions for the $S_0 \rightarrow S_1$ transition of the UV-Vis absorption spectra in solution were surprising, the latter being clearly different from formerly investigated more simple 1,7-bis-phenoxy PBIs.[23] Herein, we present a series of regioisomerically pure 1,7-substituted PBIs (Scheme 1) to gain insights into the conformational rigidity of the PBI core and the extent to which solid-state packing effects can influence the PBI scaffold geometry. Four single crystal X-ray diffraction (SCXRD) studies for PBIs with 2,6-dimethyl-, 2,6-diisopropyl- and 2,6-diphenyl-phenoxy groups at the 1,7-bay positions provide unambiguous information regarding the geometry of this important class of dyes in the solid state. Additionally, we have sought to answer why sharp vibronic transitions are observed for these dyes in solution upon attachment of substituents at the *ortho* positions of the phenoxy substituents. Here we provide experimental and computational evidence that it is not planarity, but rather rigidity of the PBI core (owing to the conformational space occupied by the phenoxy substituents in solution) that is responsible for the pronounced sharpening of the vibronically coupled optical transitions. Furthermore, we shed light on the absorption and fluorescence properties of these compounds in the solid state.

Results

Synthesis of PBIs

PBIs **4a–f** were obtained according to the synthetic route presented in Scheme 1. *N*,*N*′-Dicyclohexyl-1,7-dibromoperylene-3,4:9,10-tetracarboxylic acid bisimide (**2**)[20b] and *N*,*N*′-dicyclohexyl-3,4:9,10-tetracarboxylic acid bisimide (**4a**)[22] were synthesized according to literature procedures. On PBI **2**, isolated as a pure 1,7-regioisomer,[20b] a double aromatic nucleophilic substitution was carried out using 2,6-substituted phenol derivatives in the presence of anhydrous potassium carbonate in dry NMP at 120 °C to achieve **4b–f** in 83%, 87%, 74%, 88% and 79% yields, respectively. All new PBIs were characterized by ^{1}H NMR spectroscopy and high resolution mass spectrometry, as well as single crystal X-ray diffraction analysis for **4d–f**.

Molecular structure and packing arrangements in the solid state

Single crystals of **4d–f** were obtained upon slow evaporation of a solvent mixture at room temperature after several days and were characterized by single crystal X-ray analysis (for details see ESI†). For **4e** we were able to grow two different forms from different solvents with and without co-crystallized CH_2Cl_2 molecules. Despite our efforts, the structures still suffer from

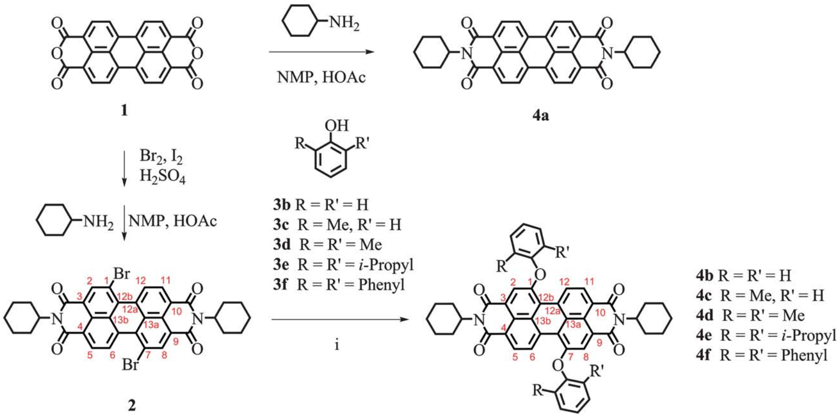

Scheme 1 Synthesis of PBIs **4a–f**: (i) anhydrous K_2CO_3, dry NMP, 120 °C, 3 h, 74–88%.

disorder of the substituents, in particular the cyclohexyl units attached at the imide nitrogens, whereas the perylene cores are well ordered in all the cases investigated here. Fig. 1 shows the molecular structures of PBIs **4d** and **4e** as found in the crystal structures. The distortion of the PBI π-scaffold was analyzed following two different approaches. In the first approach, the perylene scaffold was cut into two naphthalene subunits and the rotational twist of the averaged naphthalene planes with regard to each other was taken as the twist angle, and, in the second approach, dihedral angles were derived from the position of either the four so called "bay carbon atoms" C1, C12b, C12a, C12 (∠(C1–C12b–C12a–C12), for numbering see Scheme 1) or the four inner carbons C12a, C13a, C13b, C12b (∠(C12a–C13a–C13b–C12b), for numbering see Scheme 1; all data are collected in Table 1). Both values give very similar information, however, only the latter include the intrinsic C_2 symmetry axis of rigid molecules. Nevertheless, we also include the values of the angle including the bay carbon atoms since they have been used in many previous investigations. PBIs **4d** and **4f** present centrosymmetric molecules showing identical dihedral angles on both bay areas, whilst the symmetry is broken for PBI **4e** (both structures) resulting in two different values for the two bay areas. Table 1 shows also that the outer dihedral angles are always larger than the inner ones, which is logical because the outer side is less fixed in the polycyclic aromatic π-scaffold. It is also noteworthy that the phenoxy units are located on the same face of the perylene bisimide core for PBI **4e** (see Fig. 1d), whereas for PBIs **4d** (Fig. 1b) and **4f** (Fig. S2b in the ESI†) the phenoxy substituents are arranged on the opposing faces of the PBI core.

The two different views of PBI **4d** molecules represented in Fig. 1a and b reveal an almost planar π-scaffold, where the two phenyl substituents are almost perpendicular to the PBI core. Since the molecule lies on a centre of symmetry (space group $C2/c$, $Z = 4$), the twist angle between the two naphthalene planes is 0.0°. On the other hand, the dihedral angle between the four bay carbon atoms C1, C12b, C12a and C12, ∠(C1–C12b–C12a–C12) is 9.5(3)° and accordingly reveals significant distortion. PBI **4e** crystallized in two different forms, in one of which solvent CH_2Cl_2 is included, whereas the other one is solvent-free. Fig. 1c and d show the molecular structure of PBI **4e** that co-crystallized with CH_2Cl_2. The cell in space group $P2_1/n$ contains 4 molecules ($Z = 4$) in general positions and thus (in contrast to **4d**) gives margin to a distorted scaffold with a propeller-type twist of 15.56(9)° between the two naphthalene planes. The dihedral angles involving the four bay carbon atoms amount to 14.1(8)° and 12.2(8)°. On the other hand, the solvent-free structure of the same PBI molecule exhibits the space group $Pna2_1$. Containing 4 molecules ($Z = 4$) in general positions, this cell again gives room for a twisted molecule (see Fig. S1a and S1b in the ESI†). We find a twist angle between naphthalene planes of 9.43(5)° and dihedral angles for the four bay carbon atoms of 8.9(3)° and 10.8(3)°. Finally, the solvent-free structure of PBI **4f** crystallized in space group $P2_1/c$.[22] As in the case of PBI **4d**, the molecule lies on a center of symmetry ($Z = 4$) presenting a twist angle of 0.0° for the two involved naphthalene planes and a fairly small dihedral angle ∠(C1–C12b–C12a–C12) for the four bay region carbons of 1.5(2)° (see Fig. S2a and S2b in the ESI†). Accordingly, an almost perfectly planar PBI scaffold has been realized in this case. It is noteworthy that the different distortions found for the four 1,7-diphenoxy-PBI π-scaffolds have a negligible effect on the C–C bond lengths between the two naphthalene planes, all of them exhibiting values in the range of 1.47(2) Å. Likewise, all other bond lengths remain in a narrow range, which corroborates that the central six-membered ring involving the bay areas is the part of the molecule which is most susceptible to conformational distortions.

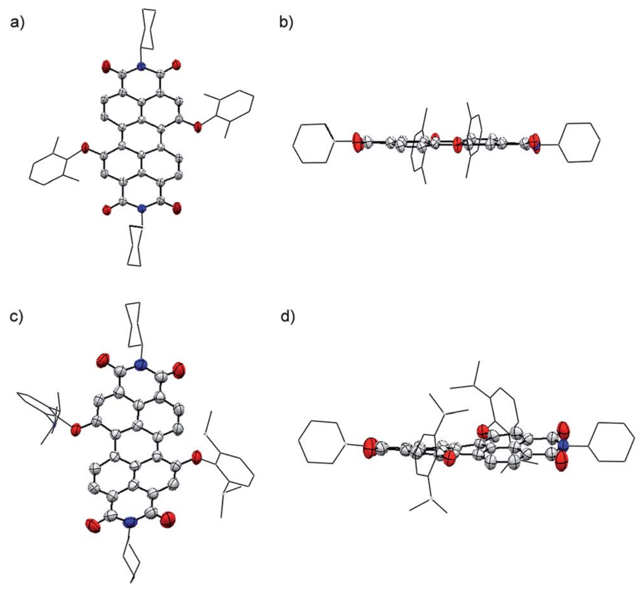

Fig. 1 Molecular structures in front view (left) and side view (right) of PBI **4d** (a and b) and **4e** (c and d). Hydrogen atoms and all solvent molecules were omitted for clarity.

The packing arrangement of PBI **4d** is characterized by two slipped stacks of strictly parallel chromophores in adjacent stacks at an angle of 75.6° (Fig. 2a). The intra-stack longitudinal and transverse offsets are considerable, and thus together with an interplanar distance of about 4 Å do not allow for overlap between the perylene π-scaffolds. Contrary to that, the molecules of PBI **4e** that co-crystallized with molecules of CH_2Cl_2 present fairly large twist angles. They instead form close pairs resulting in a two dimensional "sandwich herringbone motif" (Fig. 2c). The most remarkable feature is a slipped-stacked π-dimer unit with close π–π contacts (in the range of 3.5 Å) as pointed out by the short distance that two vicinal PBIs' "planes" present (see Fig. 2d). In the crystals of solvent-free PBI **4e** we find a completely different situation. Adjacent molecules seem "interlocked" by the *N*-dicyclohexyl substituents on either end of the perylene core, thus interlinking with each other. In this case a smaller twist angle of the perylene core was detected. We find the perylene planes fairly parallel (tilt angle 18.9°), the molecules joining a three dimensional brick wall pattern. Within the crystals of PBI **4f** we found essentially flat perylene cores forming infinite slipped stacks with no transversal but quite a considerable longitudinal offset. Both sides of the perylene planes within a

Table 1 Space groups and selected angles (°) for PBI **4d–f** according to single crystal X-ray analysis

PBI	Space group	Twist angle between naphthalene planes	∠(C1–C12b–C12a–C12)[b]	∠(C12a–C13a–C13b–C12b)[b]	Distortion along the *N*,*N*-axis
4d[a]	*C*2/*c*	0.0	9.5(3)	1.86(2)	0.0
4e[a]	$P2_1/n$	15.56(9)	14.1(8), 12.2(8)	7.5(4), 6.1(4)	4.14(5)
4e	$Pna2_1$	9.43(5)	10.8(3), 8.9(3)	4.4(2), 4.4(2)	0.54(3)
4f	$P2_1/c$	0.0	1.5(2)	0.50(1)	0.0

[a] PBI co-crystallized with CH_2Cl_2. [b] Numbering of carbon atoms are according to Scheme 1.

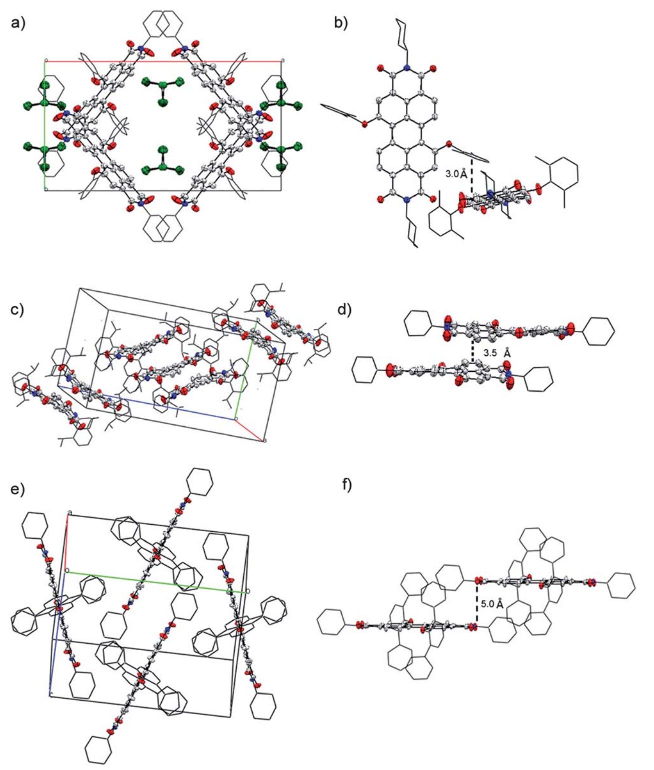

Fig. 2 Molecular packing of PBI **4d** co-crystallized with CH_2Cl_2 (a and b), PBI **4e** co-crystallized with CH_2Cl_2 (c and d) and solvent-free PBI **4f** (e and f). Hydrogen atoms were omitted for clarity.

layer seem effectively shielded by the *N*-dicyclohexyl substituents of adjacent molecules (see Fig. 2e). All the diphenylphenoxy substituents find their place at either side of the layer, successfully isolating the PBIs' cores at a distance of 5.0 Å (Fig. 2f).

Optical properties

The optical properties of the chromophores of **4b–f** were investigated by UV-Vis and fluorescence spectroscopy both in solution and solid state (Table 2). Bay-unsubstituted *N*,*N*′-dicyclohexyl-3,4:9,10-perylenetetracarboxylic acid bisimide (**3a**) was used as a reference compound.

The absorption spectra (Fig. 3a) of PBIs **4d–f** reveal sharp $S_0 \rightarrow S_1$ transitions with three well-defined vibronic progressions with maxima between 551–556 nm, 512–516 nm, and 479–483 nm in CH_2Cl_2. The higher energetic $S_0 \rightarrow S_2$ transition is observed for PBIs **4b–f** at 396 nm. Accordingly, in comparison to that of the parent PBI **4a**, a 25 nm bathochromic shift was found for PBIs **4d–f**, which is attributed to the electron-donating effect of the oxygen substituents. On the other hand, PBI **4b** reveals an almost lost vibronic pattern for the $S_0 \rightarrow S_1$ transition, while PBI **4c** presents clearly an intermediate state. Thus, the absorption maxima of PBI **4b** and PBI **4c** exhibit significantly smaller absorption coefficients (for ε values see Table 2) and are 20 and 10 nm hypsochromically shifted, respectively, to those of PBIs **4d–f**.

The fluorescence spectra (Fig. 3b) show similar progressions to their absorption data, with mirror-image vibronic patterns to the absorption spectra obtained for PBIs **4b–f** in CH_2Cl_2. Additionally, the remarkably small Stokes shifts calculated between the absorption and fluorescence maxima are noteworthy for PBI **4d** (448 cm^{-1}), PBI **4e** (445 cm^{-1}), and PBI **4f** (442 cm^{-1}), whereas PBI **4b** (984 cm^{-1}) and PBI **4c** (771 cm^{-1}) present a significantly increased shift (see Table 2) with the shift for PBI **4c** being again in an intermediate state between the values for **4d–e** and **4b**. High fluorescent quantum yields close to unity were found for all PBI derivatives.

For solid samples the situation changes entirely, pointing at the enormous impact of dye–dye interaction for this class of chromophores. This issue is most strikingly exemplified by the comparison of unsubstituted PBI **4a** (containing π-stacked molecules in the crystal)[25] or the π-stacked PBI **4e** polymorph (for packing see Fig. 2c and d) on the one hand and PBI **4f** on the other hand, which exhibits the most bulky triphenyl

Table 2 UV-Vis absorption and fluorescence properties of PBIs **4a–f** in dichloromethane at 298 K and fluorescence quantum yields in solution[a] and in the solid state (values in parentheses)[b]

PBI	λ_{abs} (nm)	ε (M^{-1} cm^{-1})	λ_{fl} (nm)	Stokes shift (nm)	$\Phi_f^{a,b}$
4a	524	83 600	544	20	100 (3)[b]
4b	537	48 900	567	30	98 (13)[b]
4c	546	56 400	570	24	99 (11)[b]
4d	551	77 300	566	15	100 (13)[b]
4e	554	74 200	568	14	100 (4, 1[c])[b]
4f	556	72 800	570	14	99 (37)[b]

[a] Relative fluorescence quantum yields were determined by applying high dilution conditions (A < 0.05) with respect to Seybold's PBI fluorescence standard,[24] error ± 2%. [b] Absolute fluorescence quantum yields in the solid state were determined with an integrating sphere. [c] Fluorescence quantum yield of PBI **4e** that co-crystallized with CH_2Cl_2 molecules.

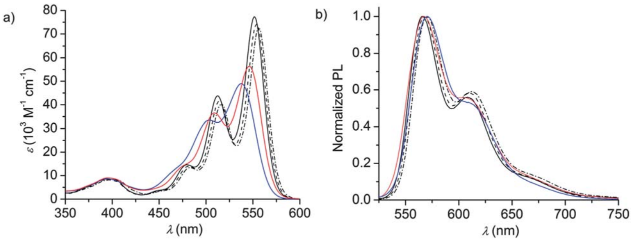

Fig. 3 UV-Vis absorption (a) and normalized emission (b) spectra of PBIs in dichloromethane: **4b** (blue line), **4c** (red line), **4d** (black solid lines), **4e** (black dashed lines), and **4f** (black dash-dotted lines) in dichloromethane at room temperature.

substituents that prohibit close π-contacts of the PBI cores in the solid state (see Fig. 2e and f). Accordingly, the UV-Vis absorption spectra of PBIs **4a** and **4b** (Fig. 4a and S9†) show the typical signatures of excitonically coupled chromophores (highest absorption coefficient for the hypsochromically displaced band, *i.e.* H-aggregate), which is attributed to closely π-stacked dyes in the solid state whilst PBIs **4d–f** show vibronic progressions similar to those found in solution (Fig. 4b and S11 and S12†), suggesting only weak interactions between the dyes in the solid state. For PBI **4c**, we note an intermediate situation according to the shape of the solid state UV-Vis absorption spectrum (Fig. S10†).

As a result of the different packing arrangements also, very different fluorescence properties are observed for solid samples of PBIs **4a–f** in contrast to the situation in solution where all of these dyes produce splendid fluorescence quantum yields of almost unity (Table 2). In the solid state, the fluorescence of **4a** (Fig. 4a) and **4e** (Fig. S12†) is almost completely quenched (quantum yields of 3% and 1%, respectively), whereas an intense fluorescence was found for PBI **4f** (37%) (Fig. 4b). Appreciable solid-state fluorescence was also found for PBIs **4b–d** with quantum yields of 13% for PBIs **4b** and **4d** and 11% for PBI **4c** (Table 2 and Fig. S9–S11†). For PBI **4e** (Fig. S12†), a slight increase of the fluorescence is observed ($\Phi_f = 4\%$) when the solid is analyzed from the solvent-free crystal polymorph, reminiscent of the parent PBI **4a** ($\Phi_f = 3\%$, red line in Fig. 4a). The impact of bulky 1,7-diphenoxy substituents is also consistent with the Stokes shifts calculated for the solid samples from the absorption and fluorescence maxima, which are large for PBIs **4a–c** (5321 cm^{-1} for **4a**, 5231 cm^{-1} for **4b**, and 4534 cm^{-1} for **4c**) and small for PBIs **4d–f** (1752 cm^{-1} for **4d**, 1337 cm^{-1} for **4e**, and 1752 cm^{-1} for **4f**).

Discussion

Properties of 1,7-diphenoxy-substituted PBIs in solution

Major information on the molecular structure of these PBIs can be derived from the UV-Vis spectra in solution. PBIs **4d–f** show very sharp bands with vibronic progressions of ~1400 cm^{-1} for the $S_0 \rightarrow S_1$ transition that indeed resemble those of the parent PBI **4a.** Likewise the absorption coefficient of the lowest energy 0,0-transition reaches a value of 77 300 M^{-1} cm^{-1} for PBI **4d** that is already pretty close to the value found for the parent dye **4a** (83 600 M^{-1} cm^{-1}). Most convincingly, the dye series **4b**, **4c** and **4d** illustrates that with each methyl group added at the phenoxy *ortho*-position, the vibronic progressions of the absorption band become sharper, giving rise to an increasing absorption coefficient at $\lambda_{\max}$, which also moves towards longer wavelengths. Moreover, the fluorescence spectra show remarkably small Stokes shifts for PBIs **4d–f** that are even smaller than those for the parent PBI **4a**, whilst those for PBIs **4b** and **4c** are considerably larger (Table 2). At first glance such changes in the spectral shape of the UV-Vis absorption bands and Stokes shift might be rationalized in terms of varying PBI core planarity. This explanation is, however, not supported by the X-ray data, which show a spread in the dihedral angles in the conformationally most flexible bay area from 0° to 15° in the single crystals of PBIs **4d–f**. Therefore, it seems rather unlikely that these molecules with almost identical optical spectra all adopt planar π-scaffolds in solution, whilst some of them are strongly distorted in the solid state.

A more reasonable explanation might be an increase of rigidity upon stepwise addition of *ortho*-substituents at the phenoxy units. To disentangle the intrinsic properties of the PBIs and the solid state effects we computed the ground state equilibrium geometry of **4a**, **4b**, and **4d–f** in the gas phase using RI-BLYP-D3(BJ)/cc-pVTZ level of theory implemented in the Turbomole 6.4 program package.[26] In addition, we computed potential energy curves (PECs) along the inner dihedral angle ∠(C12a–C13a–C13b–C12b) (for numbering see Scheme 1) by assuming C_2 symmetric molecular structures (Fig. 5) for the parent PBI **4a** and two PBIs bearing hydroxy (**4g:** *N*,*N*′-dicyclohexyl-1,7-dihydroxyperylene-3,4:9,10-tetracarboxylic acid

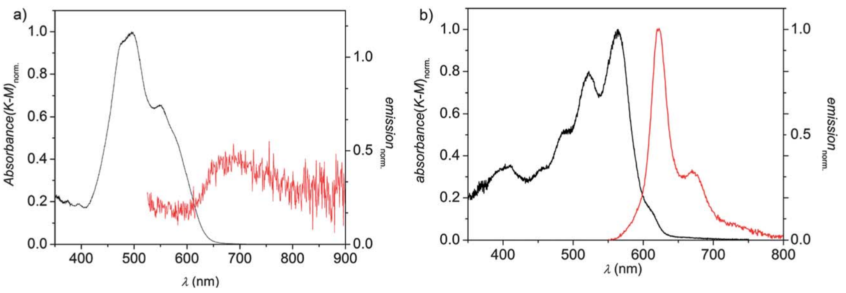

Fig. 4 UV-Vis absorption (black lines) and normalized emission (red lines) spectra of PBIs in the solid state: **4a** (a) and **4f** (b) at room temperature.

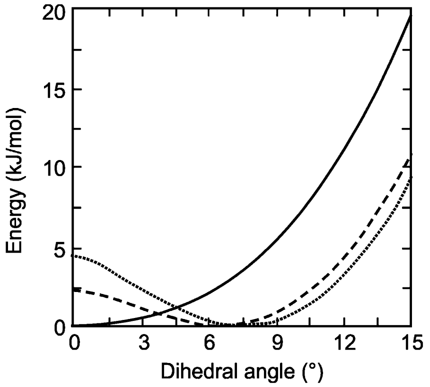

Fig. 5 ∠(C12a–C13a–C13b–C12b) bending potential energy curves (RI-BLYP-D3(BJ)/cc-pVTZ) for PBIs: **4a** (solid line), **4b** (dotted line) and **4g** (dashed line).

bisimide) and phenoxy (**4b**) substituents at the 1,7-bay positions (for details see ESI†).

The calculations for the parent PBI dye **4a** are of relevance due to the ongoing discussion if these dyes are indeed planar in solution as is commonly assumed based on dozens of crystal structures that show planar scaffolds.[27] Crystallographic data may, however, be misleading due to packing effects and because small dihedral angles of ∼2° might be hidden within thermal ellipsoids determined from single crystal X-ray analysis. In an interesting recent study, Langhals and Kinzel attributed the large temperature-dependent changes of the UV-Vis spectra of these dyes in chloroform solution to the twisted ground state populations.[28] Simple AM1 calculations by these authors suggested that the planar structure is the global energy minimum but predict a second twisted minimum that is 29 kJ mol^{-1} higher in energy. As shown in Fig. 5, our BLYP-D3/cc-pVTZ[29–31] calculations confirm that the lowest energy conformation of PBI **4a** is the planar structure but do not provide evidence for a second minimum with twisted conformations. The DFT results for **4a** and **4g** are confirmed by SCS-MP2/cc-pVTZ[32,33] computations (Tables 3 and S1†). Both approaches predict rather shallow PECs. Using the BLYP/cc-pVTZ approach, the potential energy increases by less than 3 kJ mol^{-1} for dihedral angles <7°. The flat shape of the potential is supported by SCS-MP2/cc-pVTZ computations which predict an even smaller value of 2 kJ mol^{-1} (Table S1†). Therefore, even in the absence of a second energy minimum, twisted conformations become more and more populated upon increasing temperature, which might explain the observed spectral changes in the UV-Vis spectra.

Table 3 Characterization of the ∠(C12a–C13a–C13b–C12b) bending potentials for PBI **4a**, **4b**, **4d–g** using BLYP-D3(BJ)/cc-pVTZ

PBI	∠(C12a–C13a–C13b–C12b) (°) BLYP-D3(BJ)	Energy required for planarization (kJ mol^{-1}) BLYP-D3(BJ)
4a	0.0	0.00
4b	7.6	4.3
4d	7.2	—
4e	7.1	—
4f	8.9	—
4g	6.6	2.2

Upon attachment of hydroxy (**4g**) or phenoxy (**4b**) groups at the 1,7-positions, the situation clearly changes. Gas phase RI-BLYP-D3(BJ)/cc-pVTZ predicts the minima of the PECs for ∠(C12a–C13a–C13bC12b) to be about 6° and 9° for **4g** and **4b**, respectively. Similar values were also obtained for PBIs **4d–f** (Table 3), ruling out any special effect of the *ortho*-substituents on the conformational preference of the PBI scaffold. However, like for PBI **4a**, the PESs of **4b** and **4g** are rather shallow and less than 2–5 kJ mol^{-1} is needed for the planarization of the molecules (Fig. 5 and Table 3). Hence, at room temperature, a snapshot picture of an ensemble of these molecules in solution would show scaffolds whose distortion ranges from 0 to 15° for the inner carbons owing to the Boltzmann distribution. Due to these flat bending potentials, data from single crystal X-ray diffraction analyses cannot be transferred to the situation in solution because packing effects are known to compensate for distortional energies of up to about 15 kJ mol^{-1} (there are even examples known with twice this value).[10] It is noteworthy here to point out that according to our calculations the outer dihedral angles ∠(C1–C12b–C12a–C12), *i.e.* for the bay area, are always about twice as large as the inner dihedral angles ∠(C12a–C13a–C13b–C12b) as experimentally observed in the crystal structures of the core-twisted derivatives (Table 1).

According to our theoretical analysis, all 1,7-oxy-substituted PBIs **4b–g** exhibit the lowest energy conformation at inner dihedral angles of about 7° irrespective of the substituents (hydrogen in **4g** and various phenoxy groups in **4b–f**). This value correlates with angles of about 14° if the outer dihedral angles are employed. Therefore, the question on the origin of the sharpening of the vibronic progressions in the UV-Vis absorption spectra upon attachment of substituents at the *ortho*-positions of the phenoxy groups remains to be answered. Such an effect could result since the functionalisation restricts the available conformational space of the phenoxy substituents around the dihedral angle ∠(C12b–C1–O–C14). The restriction of conformational space is expected to have a significant impact on the +M effect of the 1,7-oxygens that is responsible for the bathochromic shift of the PBI $S_0 \rightarrow S_1$ transition by up to 32 nm (**4f**) compared to PBI **4a** (Table 1 and Fig. 3) as illustrated in Scheme 2.

As indicated in Scheme 2, a positive mesomeric effect between the electron-rich oxygen substituent and the electron-poor PBI core is given. Because one of the two oxygen lone pairs is involved in CH···O hydrogen bond interactions (see subsequent paragraph), the remaining one will distribute its +M effect between either substituent, *i.e.* PBI or phenyl and this happens obviously in a rather conformation-dependent manner as observed previously for tetraphenoxy-substituted PBIs (which always exhibit strongly twisted PBI scaffolds).[5k,34] Obviously, the strongest +M effect is exerted for the most rigidified molecules, which pinpoints the concept of rigidification to control the optical properties of this class of dyes.

To substantiate our view about the restriction of flexibility, we simulated variations in the flexibility in the series **4b**, **4c** and **4d**, since between these compounds the largest deviations in

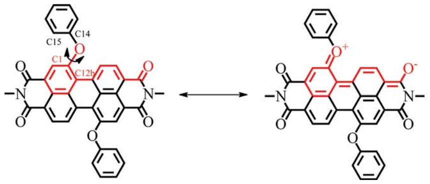

Scheme 2 Schematic representation of mesomeric structures where the +M effect of the oxygen is strongly dependent on the conformation of the phenoxy group with respect to the PBI scaffold.

the absorption spectra are found. To take the expected dependencies between ∠(C12b–C1–O–C14) and ∠(C1–O–C14–C15) (for numbering, see Scheme 2) into account we computed two-dimensional potential energy surfaces. They depend on both dihedral angles while all other parameters are optimized for each point of the surface. Additionally, we performed a molecular dynamics (MD) simulation in which all degrees of freedom can freely move according to the computed forces. All calculations are based on the semi-empirical PM6-DH2 method (see ESI†).[35] Exemplarily, Fig. 6 gives the computed two-dimensional potential energy surface as contour maps. The green dots mark the values of ∠(C12b–C1–O–C14) and ∠(C1–O–C14–C15) for each 10th time step of the respective MD simulation.

The computed two-dimensional potential energy surfaces of the three systems agree qualitatively. All exhibit two minima running parallel to each other. The orientation of both minima with respect to ∠(C12b–C1–O–C14) and ∠(C1–O–C14–C15) reflects the strong correlation between both torsional motions. Two minima (black areas) arise since a given substituted phenyl group can perform its torsion/rotation motion in two orientations. They lead to nearly identical energies since the relative distances to other atoms are nearly the same.

The surfaces agree qualitatively. However, the decreased flexibility in the series **4b**, **4c**, and **4d** is reflected in the size of the black area of the minima which strongly shrinks along the series. For compound **4b** (Fig. 6, upper part) both minima extend by about 280° for ∠(C12b–C1–O–C14) and about 260° for ∠(C1–O–C14–C15) (please note the periodic nature of the potential). For **4c** the sizes of the minima shrink to approximately 220° and 200° for ∠(C12b–C1–O–C14) and ∠(C1–O–C14–C15), respectively, while for **4d** a further restriction could be seen. These decreases in the sizes of the minima are reflected in the MD simulations.

The values of ∠(C12b–C1–O–C14) and ∠(C1–O–C14–C15) for each 10th time step are indicated by green dots on the surfaces. For **4b** we find no rotation around ∠(C12b–C1–O–C14) (around the complete phenoxy group) but as indicated by green crosses in both minima, a rotation around ∠(C1–O–C14–C15) (around the phenyl group) takes place during our simulation. However, we only observed one complete rotation in the whole simulation, indicating that this rotation is strongly restricted. As indicated by the green crosses for **4c**, no rotation takes place and the motion is already restricted to ∠(C1–O–C14–C15) with values in the range between 170° and 320°. For **4d** the range further shrinks to 220°–310°.

These conclusions with regard to molecular rigidity are also supported by the analysis of the proton chemical shifts of bay protons 6 and 12 for PBIs **4c–f** (Table 4). The chemical shifts displayed by the 6,12-bay protons are between 9.22 and 9.87 ppm for PBIs **4c–f**, whereas those resonances appear at 8.64 ppm[25] for the parent non-substituted **4a**. Fig. 7 shows how the chemical shifts corresponding to the aromatic protons of PBIs **4b–d** move downfield with increasing number of *ortho*-methyl substitutents, suggesting the presence of C–H⋯O hydrogen bonds. Concomitant to the involvement of H^6 and H^{12} protons in hydrogen bonding, displacements to higher fields were found for the H^2 and H^8 protons that are located in direct proximity to the respective phenoxy substituents. Also, this displacement directly correlates with the number of *ortho*-methyl substituents, *i.e.* 8.27 ppm (**4b**, no methyl), 8.08 ppm (**4c**, one methyl), and 7.89 ppm (**4d**, two methyl groups). Such a phenomenon is consistent with an increasing ring current effect imposed by the phenoxy groups on the proximal hydrogens concomitant with the rigidification. Remarkably, for PBI **4e** bearing the more bulky isopropyl substituents at the *ortho*-positions, identical (H^6, H^{12} and H^5, H^{11}) and very similar (H^2, H^8) chemical shift values for the proton resonances are observed as for PBI **4d**, corroborating similar conformation and rigidity. In contrast, significant deviations are found for the PBI aromatic proton resonances of *ortho*-phenyl substituted PBI **4f** compared with the alkyl-substituted analogues. For PBI **4f** we assume an equally strong CH⋯O bond. However, additional effects by the four phenyl groups in terms of diamagnetic aromatic ring currents (and maybe additional C–H⋯π interactions) influence the chemical shifts of the protons H^6 and H^{12} and to a lesser extent also the other protons attached to the PBI scaffold, making conclusions with regard to conformational changes compared to **4d** and **4e** impossible. Undoubtedly, however, all of our findings corroborate the importance of rigidity induced by the fixation of 1,7-phenoxy groups by *ortho*-substituents and supported by CH⋯O hydrogen bonding for obtaining vibronically well-structured absorption bands with high absorption coefficients also for core-substituted PBIs.

Properties of 1,7-diphenoxy-substituted PBIs in the solid state

Our gas phase calculations, which consistently explain the experimental results obtained in solution, have clearly established that the lowest energy conformation of all 1,7-phenoxy-substituted PBIs **4b–f** is characterized by twisted PBI π-scaffolds with dihedral angles of about 7° for the inner ring. This is in contrast to the experimentally observed spread in our single crystal data (Table 1), which ranges from 0.5° (**4f**) *via* 1.9° (**4d**) and 4.4° (**4e**) up to 7.5° (**4e**). These variations have obviously to be attributed to packing effects which appear in most cases to compress the molecules into more planar geometries. The only exception is the **4e** polymorph bearing a slipped π-stack dimeric unit which stabilizes the twisted arrangement as similarly observed for 1,6,7,12-tetraphenoxy-PBI J-aggregates.[7,36]

Planarization of π-conjugated molecules by packing effects has been observed before for π-conjugated molecules, the most popular example being given by *para*-terphenyl and higher

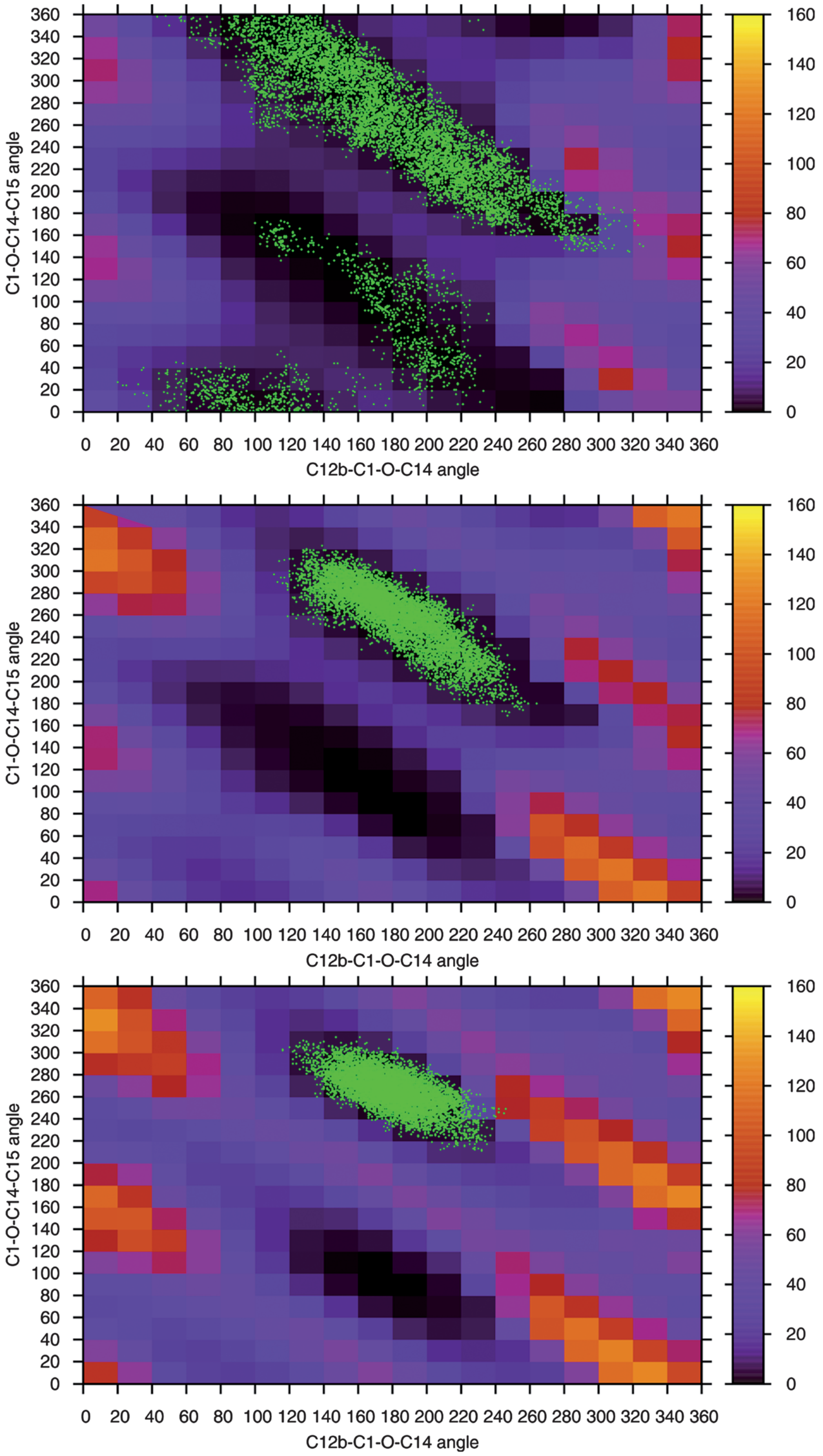

Fig. 6 Potential energy surfaces as a function of ∠(C12b–C1–O–C14) and ∠(C1–O–C14–C15) for compounds **4b** (upper), **4c** (middle), and **4d** (lower). The green dots mark the values for ∠(C12b–C1–O–C14) and ∠(C1–O–C14–C15) for each 10th time step of the respective molecular dynamics simulation. Angles are given in (°), the color code represents energy in kJ mol^{-1}. Please note the periodicity of the surface, *i.e.* after 360° the surface starts again at 0°.

homologue *para*-oligophenyl compounds.[37] Different from these examples, however, the crystals of **4d** and **4f** feature PBI scaffolds that appear as rather isolated π-planes, efficiently wrapped by the bulky phenoxy substituents at the 1,7-positions. In such cases, packing effects seem to be less important indicating that rapid oscillations between more distorted energy minima or disorder in the solid state simulate a planar structure. However, in our case we believe that the packing might

Table 4 ^1H NMR (400 MHz) chemical shifts for PBI core protons of PBIs **4b–f** measured in deuterated dichloromethane at 298 K

PBI	H^6, H^{12}/ppm (d, $J = 8.5$ Hz)	H^5, H^{11}/ppm (d, $J = 8.5$ Hz)	H^2, H^8/ppm (singlet)
4b	9.53	8.56	8.27
4c	9.66	8.54	8.08
4d	9.87	8.59	7.89
4e	9.87	8.59	7.95
4f	9.22	8.33	7.74

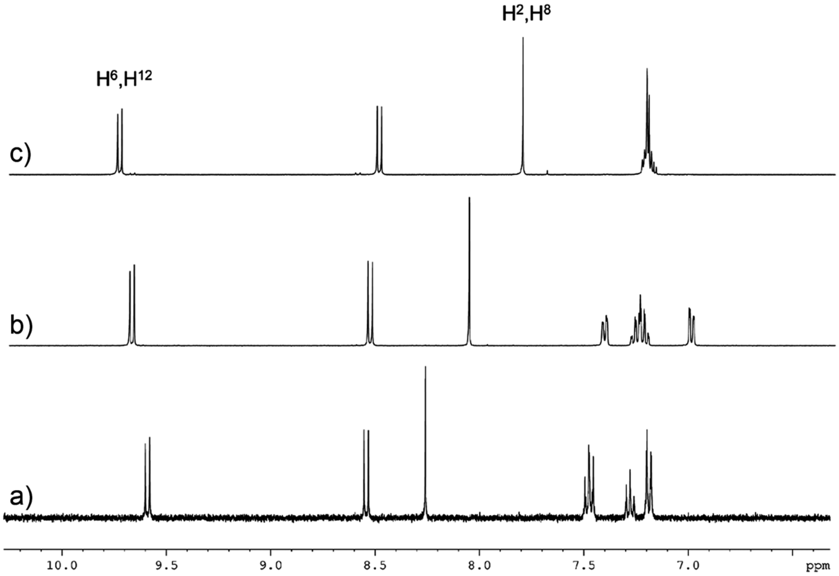

Fig. 7 Aromatic regions of ^1H NMR spectra (400 MHz, CD_2Cl_2, 298 K) for PBIs **4b** (a), **4c** (b), and **4d** (c).

indirectly induce a planar π-conjugated PBI core. To obtain some insights into such effects we performed restricted geometry optimizations (see section 5.3 in the ESI†) in which only the inner π-conjugated core is allowed to relax, while the positions of the carbon atoms of the phenoxy substituents are kept fixed at their positions measured in the X-ray experiments (see Fig. S13† for clarity). The results are gathered in Table 5 (please note that for **4e** we took the data obtained for the co-crystallization with CH_2Cl_2).

A comparison of the results obtained from the restricted geometry optimizations (Table 5) with those obtained from a full relaxation (Table 3) clearly confirm the indirect influence of packing effects on the planarization of inner π-conjugated PBI cores. If the complete molecule (inner and outer part) can relax, all molecules have ∠(C12a–C13a–C13b–C12b) dihedral angles around 7–9°. If, however, the positions of the outer substituents are fixed to their orientations found in the crystals, the trends found in the X-ray measurements (Table 1) are nicely reproduced.

The optical properties observed for the solid samples can be easily related to the given molecular packing arrangements. Thus, if the transition dipoles that are oriented along the long axis of the PBI scaffold are far apart from neighbouring molecules as given in the crystals of PBI **4d** and **4f** (the calculated center-to-center distances between closest PBI pairs are 13.04(2) and 7.59(2) Å, respectively), we observe absorption spectra with three well-defined vibronic progressions between 483–490 nm, 516–522 nm, and 557–564 nm, similar in shape and position to the spectra in solution. For all spectra the intensity of these three progressions increase with increasing wavelength, again in agreement with the observed spectra in solution. Although these spectra corroborate the idea that the dyes remain isolated within the solid state without significant electronic or excitonic interactions, we like to point out that at the long wavelength edge of the absorption band a shoulder is observed (Fig. 4b), the origin of which remains an open question. The other extreme case is given by PBIs **4a** and **4b**, whose solid state absorption spectra (Fig. 4a and S9†) provide clear evidence for excitonically coupled transition dipole moments which originate upon close π–π-stacking of these chromphores.[3a] Both UV-Vis spectra show the maximum centered at 510 nm (H-band), with a red-shifted shoulder (J-band) around 540 nm. Such aggregate absorption spectra resemble those found for dimer aggregates of similar PBIs in solution. For comparison, absorption maxima in solution have been observed at 511 nm for covalently fixed[38] and at 506 nm for self-assembled[39] dimer aggregates of 1,7-diphenoxy PBIs, where direct π–π contacts at distances of ~3.5 Å lead to strong excitonic coupling of the transition dipole moments giving rise to ~40 nm hypsochromic shifts in sandwich-type aggregate structures.

Table 5 Selected angles (°) for PBI **4d–f** calculated with BLYP-D3(BJ) by keeping the non-hydrogen atoms of the bay-substituents fixed at their positions given in the crystal structure

PBI	Twist angle between naphthalene planes	∠(C12a–C13a–C13b–C12b)	Distortion along the *N*,*N*-axis
4d	0.05	1.20	1.27
4e	15.50	7.18	0.02
4f	0.67	0.69	0.15

It is also known that such closely stacked dye aggregates with predominant H-aggregate character are at best weakly fluorescent[40] due to the relaxation of the exciton into the forbidden or at least only weakly allowed lower energy excitonic state.[41] Accordingly, the strongly quenched fluorescence ($\Phi_f = 3\%$) for the solid samples of PBI **4a** is well explained. Also, fluorescence quantum yields of around 10% for the other derivatives whose absorption spectra indicate predominant H-aggregate character are in line with earlier observations for such aggregates in solution where structural relaxations may lead to weakly emissive excimer species.[42] However, there are many other fluorescence quenching mechanisms that may operate in the solid state and that may lead to reduced fluorescence quantum yields. Obviously such mechanisms are given even for PBI **4d**, whose crystal structure and solid state UV-Vis spectra suggest the presence of rather isolated and only weakly coupled chromophores. Only for PBI **4f** bearing the most bulky and shielding terphenyl substituents is a significant increase of the solid state fluorescence quantum yield to 37% achieved, making this material one of the most fluorescent ones in the field of PBI solid state materials.[43,44] Such a high value can be explained by the consequent isolation of the chromophore in the solid state by the bulkiness of the phenyl groups which enwrap the PBI core.

Conclusions

In conclusion, a series of 1,7-diphenoxy-PBIs equipped with substituents of different bulkiness on one or both *ortho*-positions of the phenoxy substituents has been synthesized and investigated to clarify their impact on molecular structure and optical properties in solution and the solid state. Surprisingly, unprecedented intense, sharp, and well-defined transitions in the UV-Vis absorption spectra were found for all 1,7-diphenoxy substituted PBIs where both *ortho*-positions of the phenoxy substituent were equipped with methyl, isopropyl or phenyl groups. If only one of the two *ortho*-positions is functionalized, however, already broader absorption spectra are observed and accordingly such a molecule presents an intermediate state when compared with parent 1,7-diphenoxy PBI and derivatives where all *ortho*-positions were substituted. Quantum chemical calculations and single crystal X-ray analyses showed that these variations in the absorption spectra are not a consequence of the planarity of the PBI core but evolve from the less flexible arrangement of the phenoxy groups upon *ortho*-functionalization to give a more rigid molecular scaffold. CH⋯O hydrogen bonds appear to support the restriction of rotation of the phenoxy group with respect to the PBI core, orienting one of the free electron pairs of the oxygen atom to the adjacent hydrogen of the PBI bay region. It was also demonstrated that all PBIs exhibit fluorescence quantum yields in dichloromethane solution close to unity, indicating that the introduction of substituents at the *ortho*-positions of the phenoxy group has a negligible effect on this molecular property.

A second major theme of this study was to elucidate the structural and optical properties of these dyes in the solid state. Two single crystal structures revealed almost planar π-scaffolds, while two other structures showed torsional twists around the bay area with dihedral angles similar to those obtained with high level quantum chemical calculations for isolated molecules. Because the quantum chemical calculations also provided insight into the rather small energetic penalty of 2–4 kJ mol^{-1} to planarize these dyes, we can conclude that such energies are obviously within the energy range where packing effects may exert a significant impact on the molecular structure observed in the solid state. In contrast to the situation in solution, any substituent may have a significant impact on the UV-Vis absorption and fluorescence spectra and fluorescence quantum yields in the solid state because these properties are strongly influenced by the particular packing of the molecules. For the molecules investigated in this study we could cover a broad range of different optical properties from almost unaltered UV-Vis spectra with similar vibronic progressions as observed in solution and appreciably high fluorescence quantum yields up to strongly altered UV-Vis spectra with hypsochromically shifted absorption bands and very low fluorescence quantum yields. Such differences could be rationalized based on the molecular packing in the crystal. Thus, when the PBI π-scaffolds approached each other at close PBI–PBI contact distances the fluorescence was almost quenched, whilst for PBI scaffolds that were kept at a large distance from each other, *e.g.* by bulky 2,6-diphenylphenoxy substituents attached to the 1,7-PBI bay positions, the fluorescence remained intense. Interestingly, complete isolation of the PBI core by bulky substituents not only provided the most clean vibronic progressions and the highest fluorescence quantum yields, but also afforded almost planar π-scaffolds, while significant distortion of the PBI π-scaffold was found when longitudinally slipped PBI cores established π–π contacts.

Acknowledgements

Financial support by the DFG in the framework of the research unit FOR 1806 "Light-induced dynamics in molecular aggregates" at the University of Würzburg is gratefully acknowledged.

Notes and references

1 (*a*) *Handbook of Conducting Polymers*, ed. T. A. Skotheim, R. L. Elsenbaumer and J. R. Reynolds, Marcel Dekker, New York, USA, 1998; (*b*) K. Hunger, *Industrial Dyes*, Wiley-VCH, Weinheim, 2003.

2 (*a*) E. Clar, *Polycyclic Hydrocarbons*, Academic Press, London, 1964; vol. 1–2; (*b*) R. G. Harvey, *Polycyclic Aromatic Hydrocarbons*, Wiley-VCH, New York, 1997; (*c*) Y. Geerts, F.-G. Klärner and K. Müllen, in *Electronic Materials: The Oligomer Approach*, ed. K. Müllen and G. Wagner, Wiley-VCH, Weinheim, 1998, p. 48; (*d*) M. D. Watson, A. Fechtenkötter and K. Müllen, *Chem. Rev.*, 2001, **101**, 1267–1300; (*e*) L. Chen, Y. Hernandez, X. Feng and K. Müllen, *Angew. Chem., Int. Ed.*, 2012, **51**, 7640–7654.

3 (*a*) F. Würthner, *Chem. Commun.*, 2004, 1564–1579; (*b*) C. Huang, S. Barlow and S. R. Marder, *J. Org. Chem.*, 2011, **76**, 2386–2407; (*c*) H. Langhals, *Heterocycles*, 1995, **40**, 477–500.

4 P. Osswald and F. Würthner, *J. Am. Chem. Soc.*, 2007, **129**, 14319–14326.

5 (*a*) F. Würthner, *Pure Appl. Chem.*, 2006, **78**, 2341–2349; (*b*) R. Schmidt, J. H. Oh, Y. S. Sun, M. Deppisch, A. M. Krause, K. Radacki, H. Braunschweig, M. Könemann, P. Erk, Z. A. Bao and F. Würthner, *J. Am. Chem. Soc.*, 2009, **131**, 6215–6228; (*c*) F. Würthner, P. Osswald, R. Schmidt, T. E. Kaiser, H. Mansikkamäki and M. Könemann, *Org. Lett.*, 2006, **8**, 3765–3768; (*d*) Z. Xie, V. Stepanenko, K. Radacki and F. Würthner, *Chem.–Eur. J.*, 2012, **18**, 7060–7070; (*e*) F. Würthner, A. Sautter and J. Schilling, *J. Org. Chem.*, 2002, **67**, 3037–3044; (*f*) F. Würthner, A. Sautter and C. Thalacker, *Angew. Chem., Int. Ed.*, 2000, **39**, 1243–1245; (*g*) P. Osswald, D. Leusser, D. Stalke and F. Würthner, *Angew. Chem., Int. Ed.*, 2005, **44**, 250–253; (*h*) Z. Chen, M. G. Debije, T. Debaerdemaeker, P. Osswald and F. Würthner, *ChemPhysChem*, 2004, **5**, 137–140; (*i*) S. Leroy-Lhez, J. Baffreau, L. Perrin, E. Levillain, M. Allain, M.-J. Blesa and P. Hudhomme, *J. Org. Chem.*, 2005, **70**, 6313–6320; (*j*) M. Sadrai, G. R. Bird, J. A. Potenza and H. J. Schugar, *Acta Crystallogr., Sect. C: Cryst. Struct. Commun.*, 1990, **46**, 637–640; (*k*) P. Osswald and F. Würthner, *Chem.–Eur. J.*, 2007, **13**, 7395–7409.

6 Z. Chen, M. G. Debije, T. Debaerdemaeker, P. Osswald and F. Würthner, *ChemPhysChem*, 2004, **5**, 137–140.

7 M. Gsänger, J. H. Oh, M. Könemann, H. W. Höffken, A.-M. Krause, Z. Bao and F. Würthner, *Angew. Chem., Int. Ed.*, 2010, **49**, 740–743.

8 Y. Shi, H. Qian, Y. Li, W. Yue and Z. Wang, *Org. Lett.*, 2008, **10**, 2337–2340.

9 For some selected articles, see: (*a*) Y. Zhang, J. L. Petersen and K. K. Wang, *Org. Lett.*, 2007, **9**, 1025–1028; (*b*) A. Rajca, H. Wang, M. Pink and S. Rajca, *Angew. Chem., Int. Ed.*, 2000, **39**, 4481–4483; (*c*) M. Miyasaka, A. Rajca, M. Pink and S. Rajca, *J. Am. Chem. Soc.*, 2005, **127**, 13806–13807; (*d*) J. N. Moorthy, P. Venkatakrishnan, S. Sengupta and M. Baidya, *Org. Lett.*, 2006, **8**, 4891–4894; (*e*) W. C. Herndon, P. C. Nowak, D. A. Connor and P. Lin, *J. Am. Chem. Soc.*, 1992, **114**, 41–47; (*f*) A. J. Lovinger, C. Nuckolls and T. J. Katz, *J. Am. Chem. Soc.*, 1998, **120**, 264–268; (*g*) F. Dumitrascu, D. G. Dumitrescu and I. Aronb, *ARKIVOC*, 2010, **1**, 1, and references therein.

10 (*a*) R. A. Pascal Jr, C. M. Wang, G. C. Wang and L. V. Koplitz, *Cryst. Growth Des.*, 2012, **12**, 4367–4376; (*b*) R. A. Pascal Jr, *Chem. Rev.*, 2006, **106**, 4809–4819.

11 (*a*) S. Xiao, M. Myers, Q. Miao, S. Sanaur, K. Pang, M. L. Steigerwald and C. Nuckolls, *Angew. Chem., Int. Ed.*, 2005, **117**, 7556–7560; (*b*) Z. Wang, F. Dötz, V. Enkelmann and K. Müllen, *Angew. Chem., Int. Ed.*, 2005, **44**, 1247–1250; (*c*) S. Xiao, S. J. Kang, Y. Zhong, S. Zhang, A. M. Scott, A. Moscatelli, N. J. Turro, M. L. Steigerwald, H. Li and C. Nuckolls, *Angew. Chem., Int. Ed.*, 2013, **52**, 4558–4562.

12 (*a*) T. Schiros, S. Mannsfeld, C.-Y. Chiu, K. G. Yager, J. Ciston, A. A. Gorodetsky, M. Palma, Z. Bullard, T. Kramer, D. Delongchamp, D. Fischer, I. Kymissis, M. F. Toney and C. Nuckolls, *Adv. Funct. Mater.*, 2012, **22**, 1167–1173; (*b*) C.-Y. Chiu, B. Kim, A. A. Gorodetsky, W. Sattler, S. Wei, A. Sattler, M. Steigerwald and C. Nuckolls, *Chem. Sci.*, 2011, **2**, 1480–1486.

13 K. Mouri, S. Saito and S. Yamaguchi, *Angew. Chem., Int. Ed.*, 2012, **51**, 5971–5975.

14 Y. Hong, J. W. Y. Lam and B. Z. Tang, *Chem. Soc. Rev.*, 2011, **40**, 5361–5388.

15 D. Yokoyama, *J. Mater. Chem.*, 2011, **21**, 19187–19202.

16 C. Wang, H. Dong, W. Hu, Y. Liu and D. Zhu, *Chem. Rev.*, 2012, **112**, 2208–2267.

17 J. E. Johns, E. A. Muller, J. M. J. Fréchet and C. B. Harris, *J. Am. Chem. Soc.*, 2010, **132**, 15720–15725.

18 (*a*) S. J. Kang, J. B. Kim, C.-Y. Chiu, S. Ahn, T. Schiros, S. S. Lee, K. G. Yager, M. F. Toney, Y.-L. Loo and C. Nuckolls, *Angew. Chem., Int. Ed.*, 2012, **51**, 8594–8597; (*b*) S. J. Kang, S. Ahn, J. B. Kim, C. Schenck, A. M. Hiszpanski, S. Oh, T. Schiros, Y.-L. Loo and C. Nuckolls, *J. Am. Chem. Soc.*, 2013, **135**, 2207–2212.

19 F. J. M. Hoeben, P. Jonkheijm, E. W. Meijer and A. P. H. J. Schenning, *Chem. Rev.*, 2005, **105**, 1491–1546.

20 (*a*) A. Böhm, H. Arms, G. Henning and P. Blaschka, (BASF AG), *Ger. Pat. Appl.*, DE 19547209 A1, 1997; *Chem. Abstr.*, 1997, **127**, 96569g; (*b*) F. Würthner, V. Stepanenko, Z. Chen, C. R. Saha-Möller, N. Kocher and D. Stalke, *J. Org. Chem.*, 2004, **69**, 7933–7939.

21 (*a*) M. C. R. Delgado, E.-G. Kim, D. A. d. S. Filho and J.-L. Brédas, *J. Am. Chem. Soc.*, 2010, **132**, 3375–3387; (*b*) R. Schmidt, M. M. Ling, J. H. Oh, M. Winkler, M. Könemann, Z. Bao and F. Würthner, *Adv. Mater.*, 2007, **19**, 3692–3695; (*c*) B. A. Jones, M. J. Ahrens, M.-H. Yoon, A. Facchetti, T. J. Marks and M. R. Wasielewski, *Angew. Chem., Int. Ed.*, 2004, **43**, 6363–6366.

22 M.-J. Lin, A. J. Jiménez, C. Burschka and F. Würthner, *Chem. Commun.*, 2012, **48**, 12050–12052.

23 (*a*) M. Schneider and K. Müllen, *Chem. Mater.*, 2000, **12**, 352–362; (*b*) J. M. Serin, D. W. Brousmiche and J. M. J. Fréchet, *Chem. Commun.*, 2002, 2605–2607; (*c*) M. J. Ahrens, L. E. Sinks, B. Rybtchinski, W. Liu, B. A. Jones, J. M. Giaimo, A. V. Gusev, A. J. Goshe, D. M. Tiede and M. R. Wasielewski, *J. Am. Chem. Soc.*, 2004, **126**, 8284–8294;

(*d*) A. Perez-Velasco, V. Gorteau and S. Matile, *Angew. Chem., Int. Ed.*, 2008, **47**, 921–923; (*e*) B. Ling, Y. Zhang, Y. Wang, W. Xu and X. Li, *J. Mol. Struct.*, 2009, **917**, 133–141; (*f*) Y. Wang, H. Chen, H. Wu, X. Li and Y. Weng, *J. Am. Chem. Soc.*, 2009, **131**, 30–31; (*g*) J. Choi, C. Sakong, J.-H. Choi, C. Yoon and J. P. Kim, *Dyes Pigm.*, 2011, **90**, 82–88; (*h*) R. K. Dubey, A. Efimov and H. Lemmetyinen, *Chem. Mater.*, 2011, **23**, 778–788; (*i*) L. Perrin and P. Hudhomme, *Eur. J. Org. Chem.*, 2011, 5427–5440; (*j*) W. Jiang, C. Xiao, L. Hao, Z. Wang, H. Ceymann, C. Lambert, S. Di Motta and F. Negri, *Chem.–Eur. J.*, 2012, **18**, 6764–6775.

24 G. Seybold and G. Wagenblast, *Dyes Pigm.*, 1989, **11**, 303–317.

25 Y. Che, X. Yang, K. Balakrishnan, J. Zuo and L. Zang, *Chem. Mater.*, 2009, **21**, 2930–2934.

26 (*a*) TURBOMOLE V6.4 2012, A development of University of Karlsruhe and Forschungszentrum Karlsruhe GmbH, 1989–2007, TURBOMOLE GmbH, since 2007; (*b*) P. A. M. Dirac, *Proc. R. Soc. A*, 1929, **123**, 714–733; (*c*) S. H. Vosko, L. Wilk and M. Nusair, *Can. J. Phys.*, 1980, **58**, 1200–1211; (*d*) A. D. Becke, *Phys. Rev. A: At., Mol., Opt. Phys.*, 1988, **38**, 3098–3100; (*e*) C. T. Lee, W. T. Yang and R. G. Parr, *Phys. Rev. B: Condens. Matter Mater. Phys.*, 1988, **37**, 785–789; (*f*) K. Eichkorn, O. Treutler, H. Öhm, M. Häser and R. Ahlrichs, *Chem. Phys. Lett.*, 1995, **242**, 652–660; (*g*) K. Eichkorn, F. Weigend, O. Treutler and R. Ahlrichs, *Theor. Chem. Acc.*, 1997, **97**, 119–124; (*h*) M. von Arnim and R. Ahlrichs, *J. Chem. Phys.*, 1999, **111**, 9183–9190; (*i*) R. Ahlrichs, *Phys. Chem. Chem. Phys.*, 2004, **6**, 5119–5121; (*j*) F. Weigend, A. Köhn and C. Hättig, *J. Chem. Phys.*, 2002, **116**, 3175–3183; (*k*) E. R. Davidson, *Chem. Phys. Lett.*, 1996, **260**, 514–518.

27 (*a*) F. Graser and E. Hädicke, *Liebigs Ann. Chem.*, 1980, 1994–2011; (*b*) F. Graser and E. Hädicke, *Liebigs Ann. Chem.*, 1984, 483–494; (*c*) E. Hädicke and F. Graser, *Acta Crystallogr., Sect. C: Cryst. Struct. Commun.*, 1986, **42**, 189–195; (*d*) E. Hädicke and F. Graser, *Acta Crystallogr., Sect. C: Cryst. Struct. Commun.*, 1986, **42**, 185–198; (*e*) G. Klebe, F. Graser, E. Hädicke and J. Berndt, *Acta Crystallogr., Sect. B: Struct. Sci.*, 1989, **45**, 69–77.

28 H. Langhals and S. Kinzel, *Spectrochim. Acta, Part A*, 2011, **78**, 1212–1214.

29 A. D. Becke, *Phys. Rev. A: At., Mol., Opt. Phys.*, 1988, **38**, 3098–3100.

30 S. Grimme, J. Antony and S. Ehrlich, *J. Chem. Phys.*, 2010, **132**, 154104.

31 T. H. Dunning, Jr, *J. Chem. Phys.*, 1989, **90**, 1007–1023.

32 S. Grimme, *J. Chem. Phys.*, 2003, **118**, 9095–9102.

33 *Molecular Electronic-Structure Theory*, ed. T. Helgakar, P. Jørgensen and J. Olseen, Wiley-VCH, New York, USA, 2000.

34 E. Fron, G. Schweitzer, P. Osswald, F. Würthner, P. Marsal, D. Beljonne, K. Müllen, F. C. De Schryver and M. Van der Auweraer, *Photochem. Photobiol. Sci.*, 2008, **7**, 1509–1521.

35 M. Korth, M. Pitonák, J. Rezác and P. Hobza, *J. Chem. Theory Comput.*, 2010, **6**, 344–352.

36 Z. Xie, V. Stepanenko, K. Radacki and F. Würthner, *Chem.–Eur. J.*, 2012, **18**, 7060–7070.

37 J. L. Badour, *Crystallogr. Rev.*, 1996, **5**, 227–259.

38 T. van der Boom, R. T. Hayes, Y. Zhao, P. J. Bushard, E. A. Weiss and M. R. Wasielewski, *J. Am. Chem. Soc.*, 2002, **124**, 9582–9590.

39 Z. Chen, U. Baumeister, C. Tschierske and F. Würthner, *Chem.–Eur. J.*, 2007, **13**, 450–465.

40 (*a*) M. Kasha, H. R. Rawls and M. A. El-Bayoumi, *Pure Appl. Chem.*, 1965, **11**, 371–392; (*b*) F. C. Spano, *Acc. Chem. Res.*, 2010, **43**, 429–439.

41 R. Fink, J. Seibt, V. Engel, M. Renz, M. Kaupp, S. Lochbrunner, H.-M. Zhao, J. Pfister, F. Würthner and B. Engels, *J. Am. Chem. Soc.*, 2008, **130**, 12858–12859.

42 (*a*) Z. Chen, V. Stepanenko, V. Dehm, P. Prins, L. D. A. Siebbeles, J. Seibt, P. Marquetand, V. Engel and F. Würthner, *Chem.–Eur. J.*, 2007, **13**, 436–449; (*b*) J. M. Lim, P. Kim, M.-C. Yoon, J. Sung, V. Dehm, Z. Chen, F. Würthner and D. Kim, *Chem. Sci.*, 2013, **4**, 388–397.

43 F. Würthner, T. E. Kaiser and C. R. Saha-Möller, *Angew. Chem., Int. Ed.*, 2011, **50**, 3376–3410.

44 (*a*) S. Nakazono, Y. Imazaki, H. Yoo, J. Yang, T. Sasamori, N. Tokitoh, T. Cédric, H. Kageyama, D. Kim, H. Shinokubo and A. Osuka, *Chem.–Eur. J.*, 2009, **15**, 7530–7533; (*b*) S. Nakazono, S. Easwaramoorthi, D. Kim, H. Shinokubo and A. Osuka, *Org. Lett.*, 2009, **11**, 5426–5429; (*c*) Q. Zhao, X. A. Zhang, Q. Wei, J. Wang, X. Y. Shen, A. Qin, J. Z. Sun and B. Z. Tang, *Chem. Commun.*, 2012, **48**, 11671–11673.